PFG 2013 / 1, 0031 – 0041
Stuttgart, February 2013

Article

Introducing a Method for Spectral Enrichment of the High Spatial Resolution Images

Fakhereh Alidoost, Mohammad R. Mobasheri & Ali A. Abkar, Tehran, Iran

Keywords: spatial resolution, spectral resolution, urban environments, spectral mixture analysis, image fusion

Summary: Almost all pixels located in the urban region imaged by high/medium spatial resolution sensor systems are mixed. To resolve this problem, usually the unmixing techniques are deployed. One of the useful unmixing methods is spectral mixture analysis. It can be grouped into two parts of spectral unmixing and spatial unmixing. In this study, spectral reflectance of important urban classes is determined using spatial unmixing method. To this end, spatial information from IKONOS imagery and spectral information from Hyperion data are employed. The validity of the proposed method is substantiated through comparison of an original Hyperion image with the reconstructed image. The experimental results lead to a mean RMSE and a mean NCC of 0.03 and 0.89 respectively. In the next stage, using the extracted spectral reflectance, an image with 4 m spatial resolution and 136 bands is produced where variability of urban land covers is taken into account. It is believed that this methodology will help researcher to monitor urban change as well as urban pollution effectively.

Zusammenfassung: *Neue Methode zur spektralen Verbesserung von räumlich hoch aufgelösten Fernerkundungsszenen.* In urbanen Gebieten besitzen Fernerkundungsszenen fast ausschließlich Mischpixel. Üblicherweise werden unmixing Methoden wie die spectral unmixing analysis verwendet. Diese lässt sich in die spektrale und die räumliche Entmischung gliedern. Die vorliegende Untersuchung hat gezeigt, dass mit Unterstützung der räumlichen Entmischung die Identifizierung der spektralen Klassen städtischer Gebiete verbessert werden kann. Die Methode wurde mit IKONOS-Daten für die räumliche und Hyperion-Daten für die spektrale Information erprobt und ergab eine Genauigkeit für den RMSE von 0,03 und den NCC von 0,89. Aus beiden Datensätzen wurde eine Bildkarte mit einer GSD von 4 m und einer spektralen Auflösung von 136 Kanälen hergestellt, die sehr gut die Vielfalt der urbanen Landnutzung wiedergibt und das Monitoring von Landnutzungswandel und Umweltverschmutzung ermöglicht.

1 Introduction

There are several important un-answered questions regarding the spectral properties of urban surface materials. For instance, how do these materials differ in their spectral responses? What are the most suitable spectral bands for mapping urban land cover? What are spectral limitations of current high spatial resolution remote sensor systems in terms of mapping urban land cover?

Merging the data collected by sensors with different spatial and spectral resolutions may in many cases be a valuable tool to the analyst (Haertel & Shimabukuro 2005). Multisensor multiresolution technique (MMT) is a technique that can be applied to unmix low spatial resolution images using information regarding pixel composition extracted from co-registered high-resolution images. This makes fusion of the low and high-resolution images for synergetic interpretation possible (Zhukov et al. 1999).

High resolution remote sensing data are of special interest for a variety of applications related to urban planning and management. Hyperspectral data, on the other hand, provide extensive spectral information that can help to discriminate materials (Mobasheri & Ghamary Asl 2011) and (Herold et al. 2002).

www.schweizerbart.de
DOI: 10.1127/1432-8364/2013/0156
1432-8364/13/0156 $ 2.75

In this work, an approach that employs the linear unmixing model is used. The technique is expected to produce reflectance images with both high spectral and spatial resolution. The data used are IKONOS multispectral and Hyperion hyperspectral images in urban environments. The concept of mixed pixels, spectral mixture analysis (SMA) and MMT is discussed in section 2. Section 3 illustrates the proposed method. Study area and preprocessing steps are introduced in section 4. The experiments, results and discussion are presented in section 5. Finally, conclusions and recommendations for MMT application in urban environments are given in section 6.

2 Background

2.1 *Fraction Determination*

Some approaches determine the endmembers in mixed pixels. This is done by using the SMA technique. The equations of the SMA technique can be given by:

$$\rho'_\lambda = \sum_{i=1}^{N} f_i * \rho_{i\lambda} + \varepsilon_\lambda \qquad (1)$$

Where ρ'_λ is mixed pixel reflectance, f_i and $\rho_{i\lambda}$ are fraction and reflectance of *i*th endmember in the pixel respectively and ε_λ is the model residual taken as error involved due to the un-accounted materials as well as measurement errors. Then for determining endmember fractions, (1) can be written in a matrix form as:

$$\begin{bmatrix} \rho'_1 \\ \rho'_2 \\ \vdots \\ \rho'_m \end{bmatrix} = \begin{bmatrix} \rho_{11} & \rho_{12} & \cdots & \rho_{1n} \\ \rho_{21} & \rho_{22} & \cdots & \rho_{2n} \\ \vdots & \vdots & \ddots & \vdots \\ \rho_{m1} & \rho_{m2} & \cdots & \rho_{mn} \end{bmatrix} \begin{bmatrix} f_1 \\ f_2 \\ \vdots \\ f_n \end{bmatrix} + \varepsilon_\lambda \qquad (2)$$

where m is the number of bands, i.e. number of equations, n is the number of endmembers, i.e. number of column of the ρ matrix. The fraction of each endmember in a pixel can be calculated using the least-squares method in which the residual ε_λ is minimized. The least-squares method is subject to two constraints: all fractions are nonnegative and sum of fractions equals 1.

In a standard application of SMA, a fixed number of sample endmembers are selected and the entire image pixels are modeled by the spectra of the components of these samples. However, this procedure is limited, because the selected endmember spectra may not effectively model all elements in the image, or a pixel may be modeled by endmembers that do not correspond to the materials located in its field of view (Powell et al. 2007). Multi endmember spectral mixture analysis (MESMA) allows the number and type of endmembers to vary pixel by pixel and as a result endmember variability is taken into account.

2.2 *Determination of Class Reflectance Spectra*

The determination of the radiance (or reflectance) spectra of the classes in each mixed pixel using spectral mixture analysis is the objective of some urban research. For determining class reflectance spectra in one band and n pixels, (1) can be written as:

$$\begin{bmatrix} \rho'_1 \\ \rho'_2 \\ \vdots \\ \rho'_m \end{bmatrix} = \begin{bmatrix} f_{11} & f_{12} & \cdots & f_{1n} \\ f_{21} & f_{22} & \cdots & f_{2n} \\ \vdots & \vdots & \ddots & \vdots \\ f_{m1} & f_{m2} & \cdots & f_{mn} \end{bmatrix} \begin{bmatrix} \rho_1 \\ \rho_2 \\ \vdots \\ \rho_n \end{bmatrix} + \varepsilon_\lambda \qquad (3)$$

where ρ', f and ρ are $n \times 1$, $n \times m$ and $m \times 1$ are matrices, n is the number of pixels, i.e. number of equations, m is the number of classes and the number of column of the f matrix and ε is the model residual. A constrained least-squares method is used to retrieve spectral information (band-i reflectance) for each of the class reflectance spectra (ρ). The use of a constrained method is justified when one expects that the solution fulfils the following two conditions: 1) the radiance (or reflectance) values must be positive and 2) the radiance values cannot be larger than the radiance saturation values of low resolution sensor (or reflectance cannot be larger than 1). In these approaches, determination of class fractions for forming coefficient matrix and selection of suitable pixels are of vital importance.

In recent years Zhukov et al. (1999), Zurita-Milla et al. (2008), Zurita-Milla et al. (2009), Mezned & Abdeljaoued (2009), Haertel & Shimabukuro (2005), Zeng et al. (2007), Busetto et al. (2008), Amoros Lopez et al. (2010) and Amoros Lopez et al. (2011) used this method for determining class reflectance spectra. Subtle analysis of these works reveals that there are a few of these researches that have been focused on urban environments using this method applied to very high spatial resolution images such as IKONOS, QuickBird and GeoEye as well as hyperspectral images such as Hyperion and AVIRIS.

To apply the aforementioned equations to all bands and all pixels in the image, there are still two major problems. Firstly, the coefficient matrix (fractions matrix) may get too big. Secondly, the variability of spectra within a class cannot be found, i.e. only one spectrum can be determined for each class. To overcome these problems, different solutions are suggested. A window with certain dimension in low spatial resolution image can be used to consider class spectra variability in the whole image where the central pixel will be unmixed using characteristics of its neighbouring pixels. It is noteworthy that in this approach, window size and pixel size in low resolution imagery is important since it might produce large errors particularly for the case of urban areas.

3 Methodology

It is believed that by using high spatial and high spectral resolution imagery of the same scene, it is possible to extract spectral reflectance of sub-pixel themes. However, in this process two assumptions are made: 1) availability of relatively high spatial/spectral resolution images for the scene, 2) applicability of the linear mixing model. The technique presented in this work is named spectral enrichment of the high-spatial resolution images (SEHR). The method consists of five steps. In the first step, the high spatial resolution data are used to compute the fractional coverage of different classes present in each pixel. In the second and third steps the fractions are used to look for per-pixel endmembers reflectance spectra. In the fourth step, the extracted reflectance curves will be validated and in the final step, this information will be fused to high spatial resolution image to produce an image having both high spatial and spectral characteristics simultaneously. From this point of view, the high-resolution image is conventionally called the classifying instrument (CI), while the lower-resolution image is called the measuring instrument (MI) (Zhukov et al. 1999).

(3) is used for the determination of the class reflectance in one band and in n pixels. The SMA equation system and its constraints for the determination of reflectance spectra of each of the classes are presented in (4).

$$\begin{aligned} &P' = F.P + V \\ &\overline{P} = (F^T W F)^{-1} F^T W P' \\ &\left\{ \begin{matrix} V^T W V : \min \\ 0 \le \overline{P} \le 1 \end{matrix} \right\} \end{aligned} \tag{4}$$

Where P' is the mixed pixels reflectance matrix, F and P are the fraction and the reflectance matrices respectively, V is the model residual matrix, $\overline{P}$ is the estimated reflectance and W is the weight matrix.

As mentioned earlier, the method consists of the following operations:

1. Classification of high resolution image and extraction of the pixels class fractions.
2. Window-based unmixing of the MI-pixels for the calculation of the reflectance spectra for each class.
3. Class reflectance spectra clustering for determination of class sample reflectance spectra.
4. Validation.
5. Image fusion.

3.1 *Fraction Determination*

The high spatial resolution image is used to determine the fraction of the main class components present in the mixed pixels. In many researches (section 2), the CI image is classified using unsupervised classification technique. In this study, in order to compare the result of hard and soft classification in the MMT, the CI image is classified into *nc* classes using K-means as a hard clustering tech-

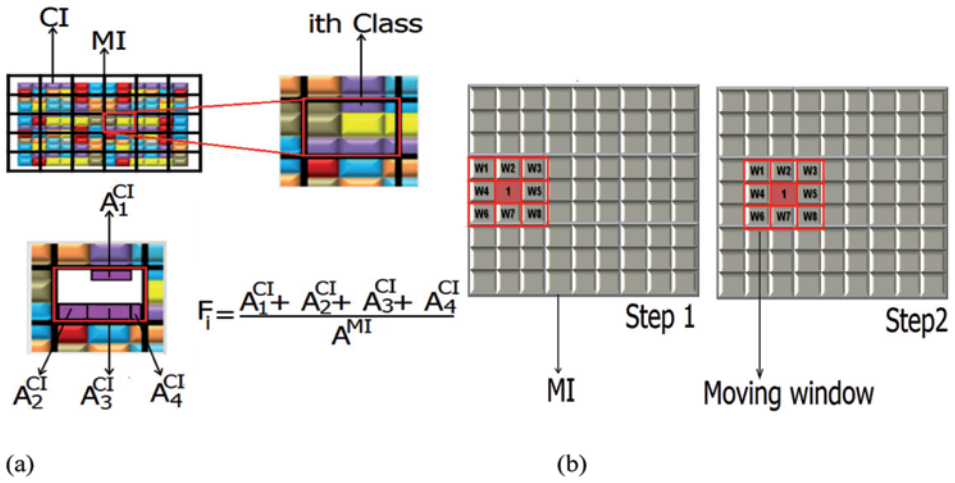

Fig. 1: (a) Fraction determination: The fractions related to each MI pixel are calculated using the area of each class; (b) Weighted moving window.

nique (MacQueen 1967) and Fuzzy C-means as a soft clustering technique (Bezdek 1981). Several *nc* values ranging from 3 to 20 are tested in this work. In this paper a novel approach is used for the determination of each class fraction in each mixed pixel. Both CI and MI images are brought to the same coordinate system. The fractions related to each MI pixel are calculated using the area of each class in one mixed pixel in the map coordinate system through (5). It is important to note that in the map coordinate system, the intersection of low and high spatial resolution pixels result in many sub-pixel regions where they have been considered in this equation (Fig. 1a). Therefore, these sub-pixels area that contributed to mixing reflectance spectra are considered in (5). In addition, the sum-to-one and non-negativity of fraction values are also satisfied.

$$f_i = \frac{\sum_{j=1}^{n} (A_j^{CI})}{A^{MI}} \qquad (5)$$

where, f_i is the fraction for ith class, A_j^{CI} is the area of jth polygon in ith class, A^{MI} is the area of a mixed pixel and n is the number of polygons in ith class.

3.2 *Calculation of Class Reflectance*

To retrieve the class reflectance spectra, the inverse linear spectral mixture analysis is used (4). The unmixing procedure for the MI pixels is performed. According to Zhukov et al. (1999), "the unmixing of the MI pixels is performed in the moving window mode". In order to unmix the central MI pixel in the window, contextual information of the surrounding MI pixels is used" (Fig. 1b). A n by n window which is moving 1 MI pixel step at a time is used in order to solve n^2 equations to unmix the central pixel. The size of selected window should be kept as small as possible so that the fused image gets spectrally consistent with the variability expected for the low spatial resolution images (Zurita-Milla et al. 2008). On the other hand, the size of this window should be sufficiently large to provide enough equations for solving the equation system. Since each system of equations results in a unique solution, the size of the selected windows should be appropriate to fulfil this task (Zurita-Milla et al. 2008). In this study, moving windows of 3 by 3 and 5 by 5 pixels dimensions are used, since high spectral variability of urban areas does not allow the use of windows of larger size. A weighted constrained least-square method is deployed for deriving the class reflectance spectra (Fig. 1b). Weights

can be calculated using spectral similarity and Euclidean distance in each window (Busetto et al. 2008). For the spectral similarity, the spectral information divergence (SID) method (Chang 1999) is used. As a result, larger weights are assigned to the pixels which are closer and more similar to central pixel in each window (6).

$$W = \frac{\text{Similarity}}{\text{Distance}} \tag{6}$$

3.3 *Determination of the Candidate Class Reflectance Spectra*

Having applied the aforementioned moving windows to MI pixels, a set of reflectance spectra for each class is derived (Fig. 2a). It is worth noting that by averaging over this set, one reflectance spectra will be assigned to each class. However, this averaging procedure misses the within-class variability. Moreover, with this averaging it becomes hard to identify the noisy spectra if one is interested in. To avoid these difficulties, as a novel approach the K-means clustering technique is used in this work. Each set of reflectance spectra for each class is clustered into ns candidate class reflectance spectra (Fig. 2b).

3.4 *Validation of the SEHR Technique*

If the class reflectance spectra and class fractions in the mixed pixels are accessible, it is possible to reconstruct the reflectance spectra of that mixed pixel using (1). However, these mixed pixels not being used in the calculation of the class reflectance spectra can be used for validation. The validity of the proposed method is substantiated through a comparison of the original mixed pixels with the reconstructed ones. As mentioned in section 3, each class has many candidate reflectance spectra and each mixed pixel contains several classes. For the reconstruction of the mixed pixel, different combinations of class reflectance spectra are mixed and tested with the original pixel reflectance spectra. The best reconstructed mixed pixel compared to the relevant original mixed pixel is selected based on minimum root-mean-square error (RMSE) values. This approach is based on MESMA technique offered by Powell et al. (2007).

The quantitative assessment is conducted by applying the RMSE, relative error (R_Error) and normalized cross correlation (NCC) (Bieniarz et al. 2011) for each reconstructed MI pixel (7, 8 & 9). Finally, the mean RMSE, mean R_Error and mean NCC for the whole reconstructed MI image are calculated.

$$RMSE_j = \sqrt{\frac{\sum_{i=1}^{n}(\rho_i^C - \rho_i^O)^2}{n-1}} \quad j = 1:N \tag{7}$$

$$NCC_j = \frac{1}{n-1}\sum_{i=1}^{n}\frac{(\rho_i^C - \rho_m^C)(\rho_i^O - \rho_m^O)}{\sigma^C \sigma^O} \quad j = 1:N \tag{8}$$

$$R\_Error_j = \left|\frac{\rho_m^O - \rho_m^C}{\rho_m^O}\right| \times 100 \quad j = 1:N \tag{9}$$

where, N is the number of reconstructed pixels, n is the number of bands, ρ_i^C and ρ_i^O stand for

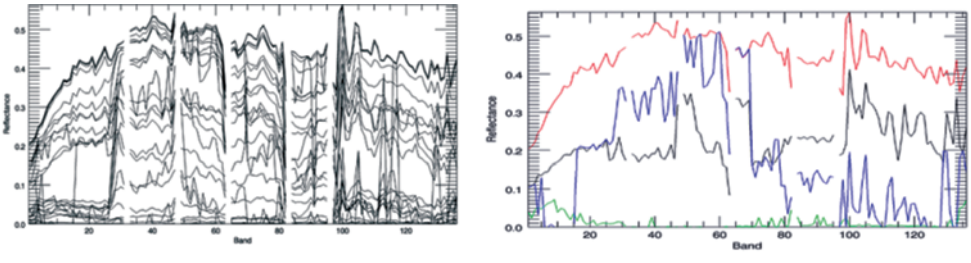

(a) (b)

Fig. 2: (a) A set of reflectance spectra for one class; (b) Candidate class reflectance spectra for same class.

reconstructed and original reflectance in *i*th band, ρ_m^C and ρ_m^O are the mean of reconstructed and original reflectance in *n* bands, (σ^C) and (σ^O) are the standard deviation of reconstructed and original reflectance in *n* bands.

3.5 *Image Fusion*

Finally, a fused image is generated by replacing each of the CI pixels by its corresponding spectral signature. This process results in a hyperspectral/high spatial resolution image with spatial/spectral variability in an urban environment. Spatial variability is addressed by allowing the type of reflectance spectra for each class to vary throughout the image. Spectral variability is addressed by allowing the number and type of spectra to vary from pixel to pixel as defined by Powell et al. (2007).

4 Datasets and Pre-processing

4.1 *Study Area*

The test area is located at Qods city in the south west of Tehran, Iran. An IKONOS MS and EO-1 Hyperion image with 4 m and 30 m spatial resolution respectively are supplied for this area (Fig. 3). This area is selected based on heterogeneity of the landscape in urban environment, cloud free condition and small difference in the acquisition time of IKONOS and Hyperion images.

4.2 *Image Pre-processing*

IKONOS Data

The IKONOS data consisted of one panchromatic image with 1 m spatial resolution and one multi-spectral image with 4 spectral bands (b/g/r/nir) and 4 m spatial resolution. It was acquired on August 29, 2004.

Geometric correction is carried out by the supplier (National Cartographic Center of Iran) using 1:2000 topographic maps through the nearest neighbour re-sampling approach.

10 and 11 are used for converting IKONOS DN data to reflectance (Taylor 2005). This preprocessing is needed for image fusion approach mentioned in the previous section.

Reflectance is defined as (Taylor 2005),

$$\rho_i = \frac{\pi L_i d^2}{E_i \cos(\theta)} \tag{10}$$

where, ρ_i is the unitless planetary reflectance, L_i is the radiance for spectral band *i* at the sensor's aperture (W/(m²·µm·sr)), *d* is the Earth-sun distance, E_i is the mean solar exoatmospheric irradiance at band *i* (W/(m²·µm)) and θ is the solar zenith angle. L_i can be obtained with the correct units from the IKONOS image product by converting from DN to radiance using (12) (Taylor 2005),

$$L_i = \frac{10^4 \times DN_i}{Calcoef_i \times bandwidth_i} \tag{11}$$

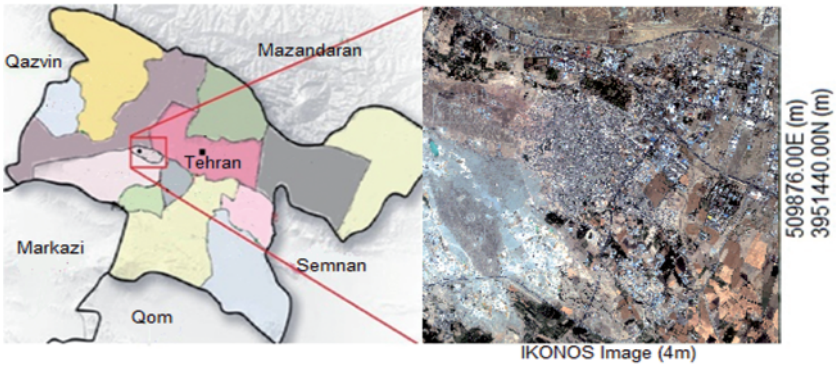

Fig. 3: Location of the study area in Qods city in the south west of Tehran, Iran.

where, $Calcoef_i$ is the radiometric calibration coefficient (DN/(mW·cm^2·sr)) and $bandwidth_i$ is the width of the spectral band *i* (nm). Both $Calcoef_i$ and $bandwidth_i$ for the IKONOS bands are given by Taylor (2005). The Earth-sun distance (d) can be obtained from any nautical handbook (Taylor 2005).

Hyperion data

An EO-1 Hyperion image acquired on August 21, 2004, around 11:00 a.m. local time is used for this study. These data are available from the USGS website with 242 spectral bands at 30 m spatial resolution.

Due to the low signal-to-noise ratio for the first few as well as the last few Hyperion spectral bands and also because of the heavy water absorption in several bands, only 196 bands were selected (bands 8 to 57 and 79 to 224). A shift of one pixel in the line direction is corrected in the SWIR image data. This shift occurs at column 128 (Staenz et al. 2002). In addition, an atmospheric correction is carried out using FLAASH in ENVI 4.7 ® software with the appropriate input data. As a result, radiance is converted to reflectance.

Geometric correction for Hyperion relative to geo-referenced IKONOS is done using 18 ground control points (GCPs) and 7 check points by the nearest neighbour re-sampling and second order of polynomial equations in PCI ® 9.1 software. The geometric errors obtained for GCPs and check points are 5.95 m and 6.63 m, respectively. However, using very high spatial resolution images, it is necessary to carry out precise registration and avoid misalignment errors. In this paper the geocoding results are adequate, showing a RMSE of 0.2 pixels. An analysis of the MMT sensitivity to sensor errors showed that the co-registration errors should not exceed 10 to 20 percent of the low-resolution pixel size (Zhukov et al. 1999).

Finally, the corrected Hyperion data with 136 appropriate bands according to EO1HS-DATA (Barry 2001) in the UTM Zone 39 N WGS-84 projection are used in this study.

5 Results and Discussion

A sample subset (30 by 30 pixels) from Hyperion image is selected as the study area. This subset corresponds to a subset (219 by 219 pixels) of the IKONOS image. Both image subsets covering the study area are shown in Fig. 4. The sample site is predominantly covered by urban structures, i.e. buildings, road, roofs, parking lots etc. The subset from Hyperion image has no bad stripes. The sample subset is divided into two parts. Part 1 is used for determination of class reflectance spectra using inverse linear spectral mixture whereas part 2 is used for validation. Hereinafter, part 1 and 2 are called the unmixing image (UI) and validation image (VI), respectively.

For an assessment purpose, four different schemes are deployed (Tab. 1). The results of mean RMSE for these four schemes are

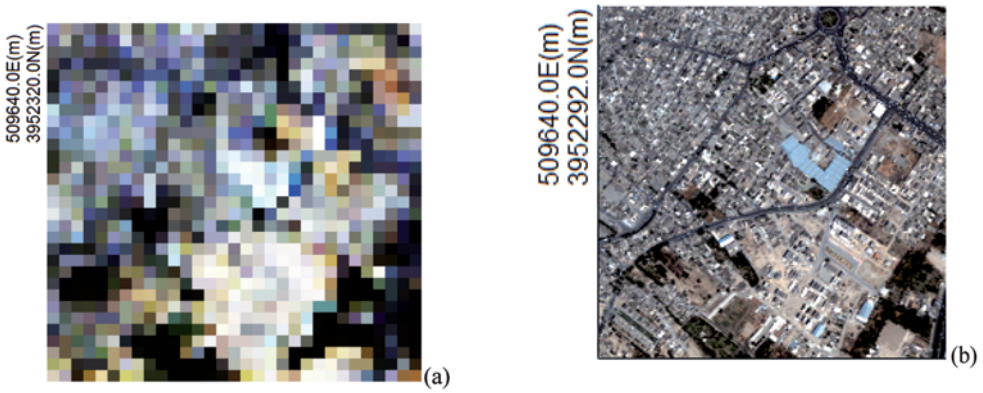

Fig. 4: The sample site, (a) Hyperion image (30 m) (30×30 pixels) and (b) IKONOS image (4 m) (219×219 pixels).

Tab. 1: The four different proposed schemes.

Scheme	Detail
1	IKONOS image classification using K-means algorithm and linear constrained least-square unmixing
2	IKONOS image classification using K-means algorithm and linear weighted constrained least-square unmixing
3	IKONOS image classification using Fuzzy C-means algorithm and linear constrained least-square unmixing
4	IKONOS image classification using Fuzzy C-means algorithm and linear weighted constrained least-square unmixing

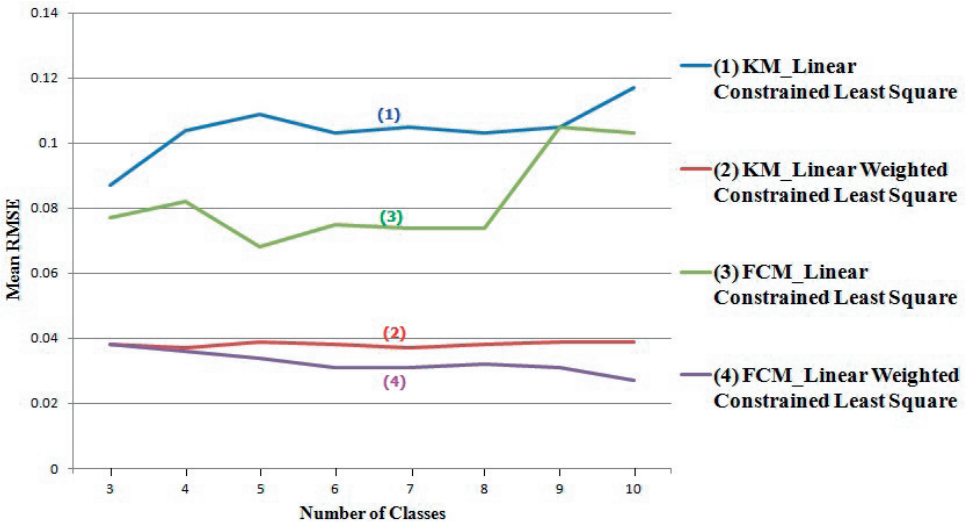

Fig. 5: The mean RMSE for four schemes.

shown in Fig. 5. It can be seen that the weighted unmixing performs better compared to unweighted unmixing. In addition, image classification by the Fuzzy C-means algorithm works better compared to the K-means algorithm (Fig. 5). So, the best results are obtained through the 4th scheme.

The classification of CI into six and ten classes has produced minimum mean RMSE (Fig. 5, curve 4). However, it should be noted that this is not a decisive result for the best number of classes in the proposed methodology because the unmixing results may vary for different conditions, like subset dimension, number of candidate reflectance spectra, moving window size and random rules in K-means clustering. Classification of IKONOS image is performed with *nc*=3 to *nc*=20 where *nc*=10 gives a minimum mean RMSE during the constrained unmixing in six runs of the method (Fig. 6). For the number of classes greater

Tab. 2: Mean errors (RMSE and R_error) and Mean NCC values between reconstructed and original Hyperion image.

10	Number of Classes
4	Maximum number of sub classes
[0.008, 0.183, 0.027]	[min, max, mean] RMSE
[0.002, 35.21, 5.00]	[min, max, mean] R_Error (%)
0.89	Mean NCC

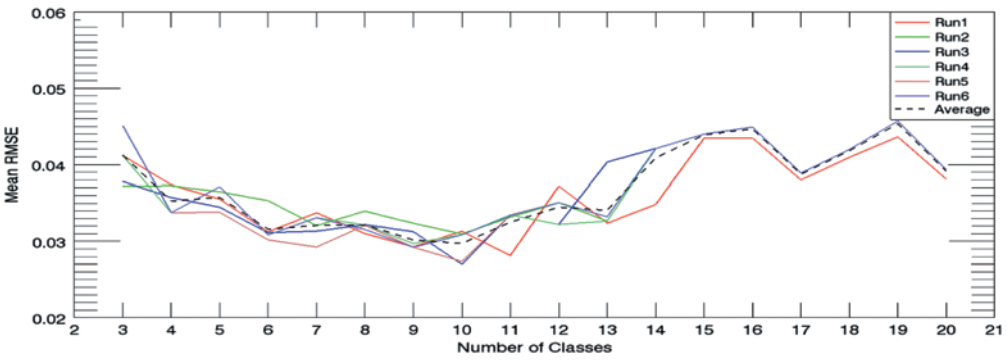

Fig. 6: The mean RMSE for the 4th scheme.

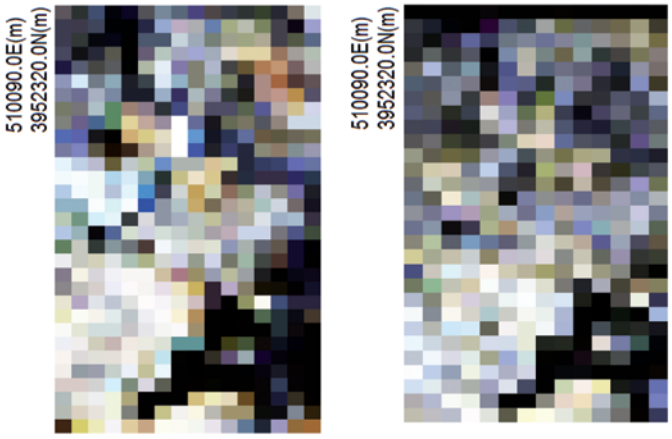

Fig. 7: (a) Original Hyperion (30 m); (b) reconstructed Hyperion (30 m).

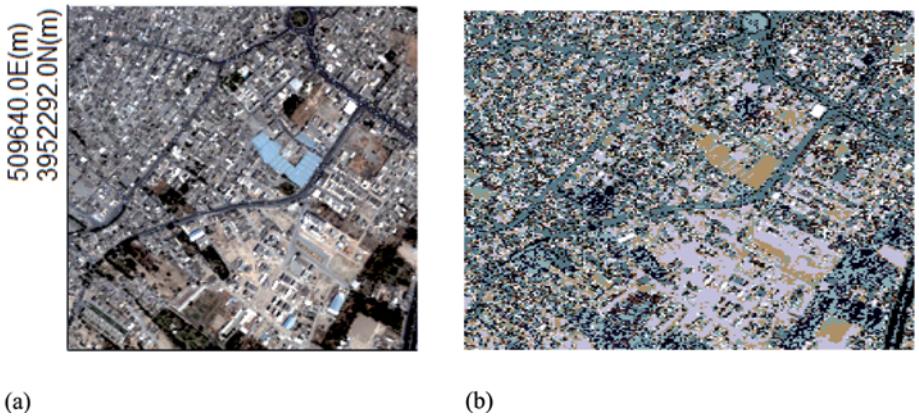

Fig. 8: (a) IKONOS image (4 m); (b) fused image (4 m).

than 9, an increase in the window size corresponds to an increase in the amount of error (Fig. 6) all due to the fact that the larger windows may have more land cover variability.

According to section 3.4, the Hyperion image is reconstructed for VI using defined candidate reflectance spectra form UI (Fig. 7). The range and mean errors (RMSE and R_error) and mean NCC values between reconstructed and original Hyperion image are depicted in Tab. 2. The results indicate that the SEHR approach is successful in retrieving urban class reflectance from the Hyperion image.

The fused image has the property of a hyperspectral image with 136 bands as well as a high spatial resolution image with 4 m pixel size (Fig. 8). It is important to notice that the accuracy of the results is influenced by the preprocessing steps. The Hyperspectral image was geo-referenced using a mathematical polynomial model. The geo-referencing results were showing a RMSE near 0.2 pixel size, i.e. 6 m. This error caused a misallocation in the fused image of about 2 pixels considering the spatial resolution of IKONOS image (4 m) and probably bad representation of the fused image due to this mis-registration. Also, the quality of the fused image is impacted by the quality of the reflectance values of the CI that is mentioned in section 3.5.

6 Conclusions

In this paper, a new approach (SEHR) for spectral enrichment of high spatial resolution images such as IKONOS was suggested. Four different schemes were designed and tested to retrieve surface spectral reflectance based on spatial unmixing processes. The technique was performed using Hyperion and IKONOS image data.

The estimated values for the spectral reflectance were evaluated by comparing the original mixed pixels to the reconstructed ones. The results showed that the IKONOS classification works better if Fuzzy C-means algorithm and linear weighted constrained least square unmixing were deployed compared to other schemes. Then, the retrieved class reflectance spectra were used to fuse a 30 m resolution hyperspectral image with 136 bands (Hyperion data) with a 4 m resolution multispectral image (IKONOS data). The fusion of the Hyperion with IKONOS datasets can be considered as a powerful technique to differentiate land cover classes. It was also found that, regardless of characteristics of different images, fusion can be carried out in feature level as well. Although SEHR was designed for IKONOS MS and Hyperion data, it can be applied to any two sets of image data. Output of this approach can be used to identify land covers, developing a spectral library of urban material, urban air pollution monitoring, exploring the parameters affecting urban reflectance changes and energy flows.

Acknowledgements

The authors wish to thank the Remote Sensing Department of K.N. Toosi University of Technology for their suggestions and support in the development of this study. Also, the authors would like to thank the anonymous reviewers for their comments on the manuscript. We also offer our appreciation to the National Cartographic Center of Iran and the User Services USGS for providing remotely sensed data.

References

Amoros-Lopez, J., Gomez-Chova, L., Guanter, L., Alonso, L. & Moreno, J., 2010: Multi-Resolution Spatial Unmixing for MERIS and LANDSAT Image Fusion. – IGARSS: 3672–3675.

Amoros-Lopez, J., Gomez-Chova, L., Alonso, L. & Guanter, L., 2011: Regularized Multiresolution Spatial Unmixing for ENVISAT/MERIS and Landsat/TM Image Fusion. – IEEE Geoscience and Remote Sensing Letters **8:** 844–848.

Barry, P., 2001: EO-1/ Hyperion Science Data User's Guide.

Bezdek, J., 1981: Pattern Recognition With Fuzzy Objective Function Algorithms. – New York, Plenum.

Bieniarz, J., Cerra, D., Avbelj, J., Reinartz, P. & Muller, R., 2011: Hyperspectral Image Resolution Enhancement Based On Spectral Unmixing And Information Fusion. – ISPRS **XXXVIII**-4/W19.

Busetto, L., Meroni, M. & Colombo, R., 2008: Combining medium and coarse spatial resolution satellite data to improve the estimation of

sub-pixel NDVI time series. – Remote Sensing of Environment **112:** 118–131.

Chang, C.I., 1999: Spectral information divergence for hyperspectral image analysis. – Geoscience and Remote Sensing Symposium, IGARSS **99**.

Haertel, V.F. & Shimabukuro, Y. E., 2005: Spectral Linear Mixing Model in Low Spatial Resolution Image Data. – IEEE Transactions on Geoscience and Remote Sensing: 2555–2562.

Herold, M., Gardner, M., Hadley, B. & Roberts, D., 2002: The Spectral Dimension in Urban Land Cover Mapping from Highresolution Optical Remote Sensing Data. – **3rd** Symposium on Remote Sensing of Urban Areas. Istanbul, Turkey.

MacQueen, J.B., 1967: Some Methods for classification and Analysis of Multivariate Observations. – **5th** Berkeley Symposium on Mathematical Statistics and Probability: 281–297, University of California Press.

Mezned, N. & Abdeljaoued, S., 2009: Unmixing Based Landsat ETM+ and ASTER Image Fusion For Hybrid Multispectral Image Analysis. – Advances in Geoscience and Remote Sensing: 407–418.

Mobasheri, M.R. & Ghamary Asl, M., 2011: Classification by diagnosing all absorption features (CDAF) for the most abundant minerals in airborne hyperspectral images. – EURASIP Journal on Advances in Signal Processing **102:** 1–7.

Powell, R.L., Roberts, D.A., Dennison, P.E. & Hess, L.L., 2007: Sub-pixel mapping of urban land cover using multiple endmember spectral mixture analysis: Manaus, Brazil. – Remote Sensing of Environment **106:** 253–267.

Staenz, K., Neville, R.A. & Clavette, S., 2002: Retrieval of Surface Reflectance from Hyperion Radiance Data. – IEEE Geoscience and Remote Sensing Symposium IGARSS **3:** 1419–1421.

Taylor, M., 2005: IKONOS Radiometric Calibration and Performance after 5 Years on Orbit. – CALCON 2005 Conference. Logan, Utah.

Zeng, Y., Schaepman, M.E., Wu, B., Clevers, J.G. & Bregt, A.K., 2007: Using Linear Spectral Unmixing Of High Spatial Resolution And Hyperspectral Data For Geometric-Optical Modelling. – ISPRS **XXXVI**/7-C50.

Zhukov, B., Oertel, D., Lanzl, F. & Reinhackel, G., 1999: Unmixing-Based Multisensor Multiresolution Image Fusion. – IEEE Transactions on Geoscience and Remote Sensing: 1212–1226.

Zhang, Y., 2002: Problems in the fusion of commercial high-resolution satellite as well as Landsat 7 images and initial solutions. – ISPRS, Commission IV, WG VII/7.

Zurita-Milla, R., Clevers, J.G. & Schaepman, M.E., 2008: Unmixing-Based Landsat TM and MERIS FR Data Fusion. – IEEE Geoscience and Remote Sensing Letters: 453–457.

Zurita-Milla, R., Kaiser, G., Clevers, J. & Schneider, W., 2009: Downscaling time series of MERIS full resolution data to monitor vegetation seasonal dynamics. – Remote Sensing of Environment **113:** 1874–1885.

Address of the authors:

Fakhereh Alidoost, M.Sc Remote Sensing, Tel.: +98-91-98667532, e-mail: f.alidoost@sina.kntu.ac.ir

Mohammad R. Mobasheri, Ph.D. Associate Professor, Tel.: +98-91-21226630, e-mail: mobasheri@kntu.ac.ir

Ali A. Abkar, Ph.D. Assistant Professor, Tel.: +98-91-21403827, e-mail: abkar@ kntu.ac.ir

Remote Sensing Department, Faculty of Geodesy and Geomatics, K.N. Toosi University of Technology, Tehran, P.O. Box: 15875-4416, Iran, Fax: +98-21-88770213.

Manuskript eingereicht: Juni 2012
Angenommen: September 2012